Texture-Based Identification and Characterization of Interstitial Pneumonia Patterns in Lung Multidetector CT

Panayiotis D. Korfiatis, Anna N. Karahaliou, Alexandra D. Kazantzi, Cristina Kalogeropoulou, and Lena I. Costaridou

***Abstract*—Identification and characterization of diffuse parenchyma lung disease (DPLD) patterns challenges computer-aided schemes in computed tomography (CT) lung analysis. In this study, an automated scheme for volumetric quantification of interstitial pneumonia (IP) patterns, a subset of DPLD, is presented, utilizing a multidetector CT (MDCT) dataset. Initially, lung-field segmentation is achieved by 3-D automated gray-level thresholding combined with an edge-highlighting wavelet preprocessing step, followed by a texture-based border refinement step. The vessel tree volume is identified and removed from lung field, resulting in lung parenchyma (LP) volume. Following, identification and characterization of IP patterns is formulated as a three-class pattern classification of LP into normal, ground glass, and reticular patterns, by means of k-nearest neighbor voxel classification, exploiting 3-D cooccurrence features. Performance of the proposed scheme in indentifying and characterizing ground glass and reticular patterns was evaluated by means of volume overlap (ground glass: 0.734 $\pm$ 0.057, reticular: 0.815 $\pm$ 0.037), true-positive fraction (ground glass: 0.638 $\pm$ 0.055, reticular: 0.942 $\pm$ 0.023) and false-positive fraction (ground glass: 0.361 $\pm$ 0.027, reticular: 0.147 $\pm$ 0.032) on five MDCT scans.**

***Index Terms*—Image segmentation, image texture analysis, respiratory system.**

I. Introduction

COMPUTED tomography (CT) has become the modality of choice for lung imaging. While high-resolution CT (HRCT) scan protocols allow visualization of fine lung structures, only a limited portion of lung parenchyma (LP) is sampled (approximately 10%) [1]. Multidetector CT (MDCT) allows acquisition of volumetric datasets with almost isotropic voxels, enabling visualization, characterization, and quantification of the entire extent of lung anatomy, thus lending its self to characterization of diffuse parenchyma lung diseases (DPLDs), often characterized by nonuniform distribution in the lung volume.

Interpretation of DPLDs is characterized by high inter and intraobserver variability, due to lack of standardized criteria in assessing its complex and variable morphological appearance, further complicated by the volume of image data reviewed [2].

Computer-aided diagnosis (CAD) schemes that automatically indentify and characterize radiologic patterns of DPLDs in CT images have been proposed to improve follow-up management decisions [1], [3]–[8]. These systems typically consist of two stages. The first stage is the segmentation of left and right LP region based up to now on gray-level methods, while the second stage performs classification of LP into normal and abnormal tissue types, exploiting 2-D [1], [3]–[6] and 3-D [7]–[9] texture analysis or gray-level thresholding [10].

In reported 3-D DPLD texture analysis schemes, nonoverlapping [7] or overlapping [8], [9] sampling volumes of interest (VOIs) of LP are utilized. In these schemes, 3-D texture analysis exploits first-order statistics [7], filter-based features [1], [4], cooccurrence matrices [7], run length matrices [7], 3-D local histograms, and fractal features [7], while classifiers, such as Bayesssian [8], neural networks [3], support vector machines (SVMs) [7]–[9], earth mover's distance, and k-nearest neighbors (k-NNs) [1] are utilized.

However, the aforementioned schemes [3]–[9] incorporate suboptimal preprocessing stages concerning lung-field (LF) and vessel-tree segmentation, required for LP identification, capable of successfully dealing with normal lung anatomy.

This paper presents a computer-aided scheme for the identification and characterization of interstitial pneumonia (IP) patterns in MDCT. The method is differentiated from previously reported schemes by employing an LF segmentation stage adapted to IP patterns (subset of DPLDs) affecting lung borders, by means of 3-D gray-level thresholding combined with a lung-border voxel classification refinement step. Furthermore, the method incorporates a robust vessel-tree segmentation method utilizing an unsupervised thresholding of responses produced by a 3-D multiscale enhancement filtering of vessels tubular structure. The identified vessel tree volume is removed from LF, to obtain the LP volume. Subsequently normal, ground glass, and reticular patterns are identified and characterized by employing k-NN voxel classification, exploiting 3-D cooccurrence analysis.

II. Materials and Methods

A. Dataset

A pilot clinical case sample was acquired consisting of 13 MDCT scans corresponding to four normal patients and

Manuscript received June 30, 2009; revised October 12, 2009. First published November 10, 2009; current version published June 3, 2010. This work was supported in part by the Caratheodory Programe (C.180) of the University of Patras.

P. D. Korfiatis, A. N. Karahaliou, and L. I. Costaridou are with the Department of Medical Physics, School of Medicine, University of Patras, Patras 26500, Grecce (e-mail: korfp@upatras.gr; karahaliou.a@med.upatras.gr; costarid@upatras.gr).

A. D. Kazantzi and C. Kalogeropoulou are with the Department of Radiology, University Hospital of Patras, Patras 26500, Grecce (e-mail: akazantzi@yahoo.gr; rat@upatras.gr).

Color versions of one or more of the figures in this paper are available online at http://ieeexplore.ieee.org.

Digital Object Identifier 10.1109/TITB.2009.2036166

ten patients diagnosed with IP secondary to connective tissue diseases, radiologically manifested with ground glass and reticular patterns. MDCT scans were obtained with a multislice (16×) CT (LightSpeed, GE), in the Department of Radiology at the University Hospital of Patras, Greece. Acquisition parameters of tube voltage, tube current, and slice thickness were 140 kVp, 300 mA, and 1.25 mm, respectively. The image matrix size was 512 × 512 pixels with average pixel size of 0.89 mm.

MDCT scans of five (out of ten) patients diagnosed with IP and MDCT scans of three normal patients were used to extract VOIs for training the k-NN classifier employed for IP pattern identification and characterization. The training set of the classifier consisted of 350 cubic VOIs (21 × 21 × 21 pixels), defined by an expert radiologist, representing patterns corresponding to reticular (150), ground glass opacities (100), and normal LP (100).

MDCT scans of the remaining five patients were used for evaluating performance of the proposed method in identifying and quantifying ground glass and reticular patterns. Furthermore, an MDCT scan of a normal patient (one out of four) was used as a control of the proposed system performance on LP identification and characterization.

B. Data Preprocessing

1) Lung-Field Segmentation: As suggested [11], LF segmentation algorithms, used as a preprocessing step in CAD schemes of lung disease, should be adapted to the specific disease pattern. In this paper, a two-stage 3-D LF segmentation technique adapted to IP patterns affecting the lung border is employed.

The first stage of the algorithm adopts a previously proposed scheme of 3-D histogram thresholding LF segmentation algorithm combined with an edge-highlighting wavelet preprocessing step [12].

However, gray-level-based thresholding algorithms are insufficient in correctly segmenting LF, in case of IPs affecting lung borders, since IPs are manifested as tissue texture alterations. To deal with LF undersegmentation, a subsequent supervised texture classification refinement stage is employed [9], [13].

Specifically, iterative neighborhood labeling of lung border voxels is performed using an SVM classifier. The SVM classifier assigns a label of LF or surrounding tissue (ST), using as inputs four first-order statistics (mean, standard deviation (SD), skewness, and kurtosis) extracted from a 7 × 7 × 7 pixel VOI centered at the voxel being labeled. Voxel labeling is initially applied on each border voxel of the initial LF volume, as provided by the 3-D gray-level-based algorithm, and subsequently, on its 18-connected neighbors. The initial LF volume is updated by adding voxels labeled as LF and removing voxels labeled as ST (muscle fat and bone). The process continues by checking every neighboring voxel of an already labeled one, until the left and right LF volumes stay unaltered. The outermost voxels of corresponding unaltered LF volumes provide the final left and right LF borders. Coordinates of already labeled voxels are stored to avoid double-checking of neighboring voxels during the LF volume updating.

2) Vessel-Tree Segmentation: Accurate segmentation of vessel tree structure is required in order to reduce false-positive detections of vessels arising from their similarity in radiologic appearance to reticular patterns. For vessel-tree segmentation, a recently proposed algorithm in pulmonary CT angiography is adopted, which exploits the tubular structure of the vessel tree [14].

Specifically, a 3-D multiscale filter is applied on the segmented LF volume to enhance vessels and vessel bifurcation points, present in the segmented LF volume, exploiting the eigenvalues of the Hessian matrix at multiple scales ($\sigma = 1, 2, \ldots, 12$ pixels). An expectation maximization algorithm is used to threshold the high response voxels at each scale, resulting in vessel segmentation. Finally, merging of vessel structure segments is performed to obtain final segmentation result.

The segmented vessel tree volume is removed from the LF volume, resulting in identification of the LP volume.

C. IP Pattern Identification and Characterization

IP pattern identification (i.e., segmentation) and characterization is achieved by subjecting LP volume to three-class voxel classification based on 3-D texture analysis. Specifically, a k-NN classifier is employed to assign a label of normal, ground glass, or reticular to each LP voxel utilizing overlapping VOI sampling.

1) 3-D Gray-Level Cooccurrence Features: The gray-level cooccurrence matrix (GLCM) [15] is a well-established tool for characterizing the spatial distribution (second-order statistics) of gray levels in an image. An element at location (i, j) of the cooccurrence matrix signifies the joint probability density of the occurrence of gray levels i and j in a specified direction θ and specified distance d from each other. The 3-D cooccurrence matrix stores the number of cooccurrences of pairs of gray levels i and j, which are separated by a distance d (in this study, $d = 1, 2, \ldots, 5$ voxels) in 13 directions of a VOI [16]. In this paper, for each distance (d) 13 3-D cooccurrence matrix features were calculated from a sliding 21 × 21 × 21 pixel VOI within the LP volume (angular second moment, contrast, correlation, variance, inverse different moment, sum average, sum variance, sum entropy, entropy, difference variance, difference entropy, information measure of correlation 1, and information measure of correlation 2). The mean and range of each feature over the 13 cooccurrence matrices (corresponding to 13 directions) was calculated, comprising a total of 26 GLCM-based features for each distance d. In total, 130 features were calculated per VOI.

2) Feature Selection: A statistical approach, the stepwise discriminant analysis [17] (SDA) is employed to reduce the dimensions of the feature vector (130).

3) k-NN Classifier: NN classification is one of the simplest supervised classification techniques in the field of statistical pattern recognition. In the present study, a k-NN classifier [1], [18] was used to assign to each LP voxel a label of normal, ground glass, or reticular, using as inputs the set of selected texture features. The k-NN classifies an unknown pattern according to the majority vote of its k-NNs. In this paper, the Euclidean distance was used as criterion. The number of neighbors (k) was selected

based on the maximum correct classification rate, using a ten-fold cross-validation method. The classifier training dataset is partitioned into ten subsamples. Of the ten subsamples, one is retained as the testing sample, while the remaining nine subsamples are used as training data. The results from the ten folds are averaged to produce the generalized classification rate. A maximum rate of 0.932 ± 0.004 was achieved, for $k = 10$ NNs.

Prior to classification, features were normalized to zero mean and unit variance. The parameters of the normalization were used to normalize the feature vector of an unknown pattern.

D. Performance Evaluation Metrics

The performance of the proposed method in identifying and characterizing ground glass and reticular patterns was evaluated by means of volume overlap (VO), false-positive, and false-negative fraction on five MDCT scans (total of 700 slices).

For this purpose, a second radiologist with expertise in CT image interpretation, defined the voxel-exact ground truth for ground glass and reticular patterns by generating manual outlines within the segmented LP.

For manual delineation, a tablet (Wacom Intuos3 Tokyo, Japan) was used with an active area of 305×305 mm with resolution of 0.2 lp/mm (lines per millimeter) and accuracy of ± 0.25 mm.

The metric of VO between "ground truth" (O), as defined by the second radiologist and computer (C)-derived borders, is given by [8], [9] as follows:

$$\mathrm{VO} = \frac{O \cap C}{O \cup C}. \tag{1}$$

To further quantify the fractions of the segmented results included or excluded with respect to the ground truth, the true-positive fraction (TPF) and the false-positive fractions (FPFs) are also calculated [14]. They were defined as:

$$\mathrm{TPF} = \frac{O \cap C}{O} \tag{2}$$

and

$$\mathrm{FPF} = \frac{O \cup C - O}{O}. \tag{3}$$

Accurate segmentation is characterized by high TPF and low FPF. The value of VO is bound between zero (no overlap) and one (exact overlap).

III. Results

Fig. 1 provides an application example of the proposed two-stage 3-D LF segmentation method. Fig. 1(a) and (b) provides segmentation results obtained from the first stage of the LF segmentation algorithm (3-D histogram thresholding combined with edge-highlighting wavelet preprocessing step). Fig. 1(c) and (d) depicts segmentation results after application of the border refinement step. Segmented LF is depicted by cyan overlay in 3-D representation [see Fig. 1(a) and (c)] and corresponding axial slice [see Fig. 1(b) and (d)]. As it is observed, LF undersegmentation, due to the presence of reticular patterns affecting lung border [see Fig. 1(b), white arrow], has been corrected by the border refinement step.

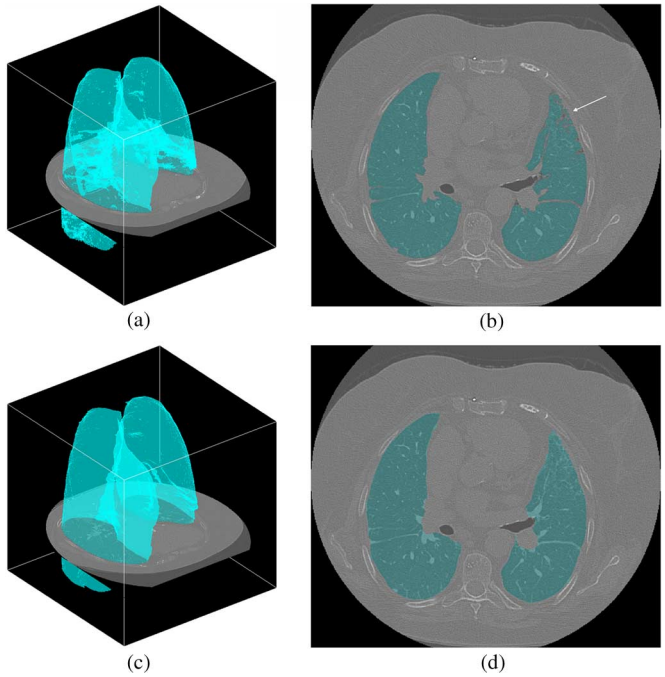

Fig. 1. LF segmentation example. (a) 3-D representation and (b) corresponding axial slice of segmented LF, provided by the first stage of the algorithm. (c) 3-D representation and (d) corresponding axial slice of segmented LF after application of the border refinement step. Segmented LF is depicted by cyan overlay. White arrow indicates LF undersegmentation (2b).

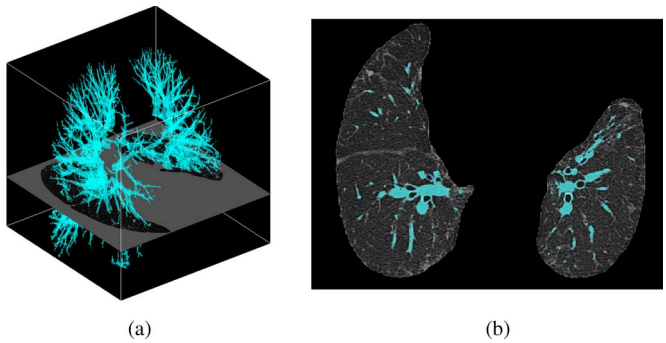

Fig. 2. Example of vessel-tree segmentation. (a) 3-D representation and (b) corresponding axial slice of the segmented vessel tree depicted with cyan overlay.

Fig. 2 depicts an application example of the vessel-tree segmentation algorithm of the case depicted in Fig. 1. Segmented vessel tree is depicted by cyan overlay in 3-D representation [see Fig. 2(a)] and corresponding axial slice [see Fig. 2(b)].

Table I summarizes the ten selected features and their corresponding numerical values (mean $\pm$ SD) for each class, provided by the SDA methodology, for varying distances d.

Fig. 3 provides an application example of the proposed IP pattern identification and characterization scheme in axial (a, b), coronal (c, d), and sagittal (e, f) planes. Green and yellow overlays correspond to ground glass and reticular patterns, respectively, while the unlabelled area corresponds to normal LP and vessel tree structures. As it is observed, both ground glass and reticular patterns have been correctly identified by the proposed

TABLE I
MEAN AND SD VALUES OF THE SELECTED TEXTURE FEATURES FOR NORMAL, GROUND GLASS, AND RETICULAR PATTERNS

Distance *(d)*	Features	Normal (mean±std)	Ground Glass (mean±std)	Reticular (mean±std)
1	Mean Contrast	268.918±40.622	209.038±58.122	401.847±50.224
	Mean Correlation	0.125±0.057	0.336±0.174	0.247±0.105
	Mean Variance	155.726±29.363	173.578±75.152	272.548±70.255
	Range Sum Average	0.265±0.186	0.547±0.373	0.533±0.268
2	Mean Sum Entropy	1.828±0.037	1.780±0.089	1.815±0.214
	Mean Variance	298.251±49.325	269.991±75.486	498.724±124.417
	Range Difference Entropy	0.037±0.025	0.061±0.0483	0.061±0.037
3	Mean Difference Entropy	1.554±0.036	1.519±0.066	1.598±0.153
4	-	-	-	-
5	Mean Correlation	0.017±0.0036	0.053±0.0075	0.280±0.0469
	Mean Difference Entropy	1.558±0.036	1.536±0.0678	1.614±0.136

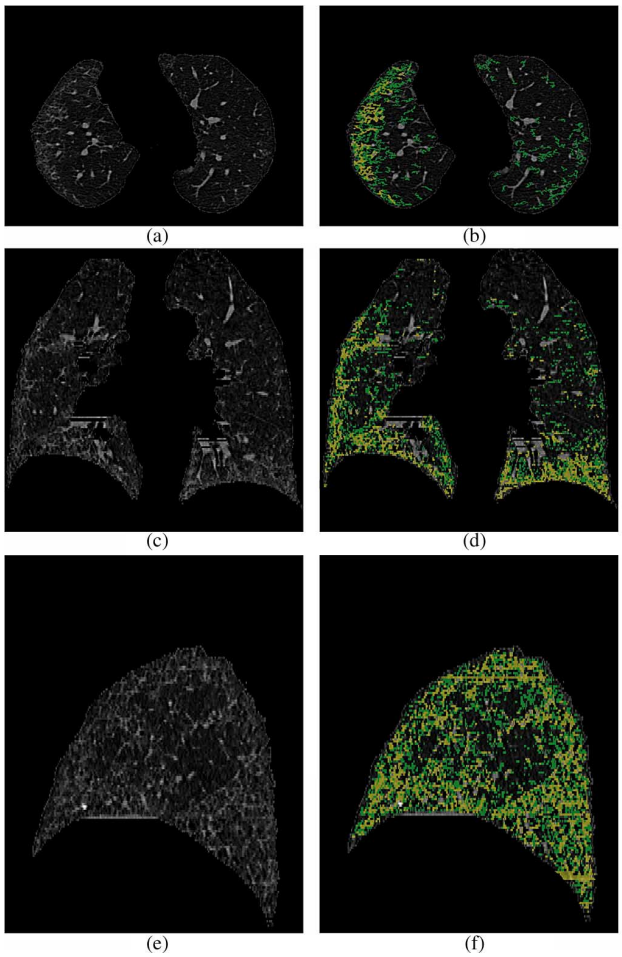

Fig. 3. Application example of the proposed method on a case including both ground glass and reticular patterns in (b) axial, (d) coronal, and (f) sagittal representation. Yellow and green overlays correspond to reticular and ground glass patterns respectively. (a) Original axial, (c) coronal, and (e) sagittal slice data are also provided.

scheme. The successful segmentation of the vessel tree, a challenging task due to radiologic appearance similar to vessels, has further contributed in improved reticular pattern identification.

Fig. 4 provides an axial plane representation of the proposed system applied on a patient with normal lung parenchyma. Green and yellow overlays correspond to ground glass and reticular patterns false positives, respectively, while the unlabelled area corresponds to normal LP and vessel tree structures.

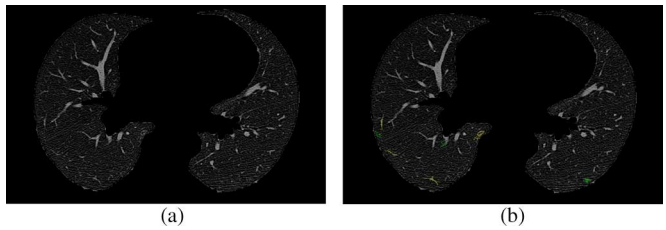

Fig. 4. Application example of the proposed method on a patient with normal LP in axial representation. Yellow and green overlays correspond to reticular and ground glass false-positive indications, respectively. (a) Original axial slice data are also provided.

Table II summarizes the performance evaluation results of the proposed system in terms of VO, TPF, and FPF for the reticular and ground glass patterns. Results are reported by mean and SD values for the five MDCT scans used for evaluation.

The performance is improved when the refinement step is applied for both ground glass and reticular patterns. The improvement was statistically significant ($p < .0001$) in case of reticular pattern for all evaluation metrics considered.

The proposed system demonstrated an improved performance in identifying and characterizing reticular patterns as compared to ground glass patterns reflected by all performance evaluation metrics.

IV. DISCUSSION

In this study, a system for the automated identification and characterization of IP patterns in MDCT is presented. Use of 3-D data enabled application of 3-D texture analysis, by means of 3-D cooccurrence features capable of capturing presence and extent of IP patterns, such as ground glass and reticular.

Identification and characterization of IP patterns is formulated as a three-class supervised pattern classification problem of LP into normal, ground glass, and reticular classes, using a k-NN classifier and a set of ten 3-D cooccurrence features, selected with SDA.

Accurate LF segmentation is an important initial step in IP identification and characterization, as diseased areas attached to lung borders may not be included in subsequent texture analysis. In this paper, LF segmentation was achieved by

TABLE II
PERFORMANCE EVALUATION RESULTS FOR GROUND GLASS AND RETICULAR PATTERNS IN TERMS OF MEAN AND SD VALUES (MEAN ± SD) OF VO, TPF, AND FPF FOR THE DATASET ANALYZED

Pattern	Segmentation	VO	TPF	FPF
Ground Glass	with refinement	0.734±0.057	0.638±0.055	0.361±0.027
	without refinement	0.713±0.064	0.623±0.044	0.353±0.031
Reticular	with refinement	0.815±0.037	0.942±0.023	0.147±0.032
	without refinement	0.694±0.087	0.765±0.076	0.097±0.063

3-D gray-level thresholding, combined with an edge-highlighting step [12], followed by 3-D first-order statistics-based border refinement [13]. Lung-field segmentation methods proposed for normal lung fields or lung field affected by juxta-pleura nodules will fail to produce accurate segmentation results because they are mainly based on gray-level thresholding. Lung-field segmentation schemes dealing with diffuse pathologies proposed up to now (Korfiatis *et al.* [13], Sluimer *et al.* [19]), both ought their accuracy to a texture analysis refinement step while utilizing different initialization (atlas and gray-level-based initializations). Table II demonstrates the improvement obtained after application of the refinement step, and especially, the impact of accurate segmentation in reticular pattern identification and quantification.

Accurate vessel-tree segmentation in DPLD analysis is a challenging task, further complicated by the presence of reticular patterns, which make conventional gray-level thresholding techniques, proposed up to now, inadequate to deal with this task [8]. Undersegmentation or oversegmentation of the vessel tree can lead to false-positive and false-negative pattern identification, respectively. The performance of the proposed method for IP pattern identification and characterization is evaluated in terms of VO, TPF, and FPF metrics. Although a direct comparison of the method performance with previously reported studies [7]–[9] is not feasible, due to lack of available reference datasets, results in terms of VO are promising [8], [9].

The relatively high performance of the proposed system (see Table II) is attributed to both the optimized data preprocessing step (LF and vessel-tree segmentation), as well as to the 3-D texture-based voxel classification approach of the LP. Specifically, accurate LF segmentation, especially in border areas affected by reticular patterns (see Fig 3), as well as the accurate vessel-tree segmentation have resulted in reduced FPF in IP pattern identification. Use of the SDA-feature-selection methodology resulted in 3-D texture features (see Table I) capable of capturing micro and macrotexture properties of IP pattern radiological manifestations and to correctly differentiate them from normal LP.

As shown in Table II, the proposed approach achieves improved performance for identification and characterization of reticular as compared to ground glass patterns. Systems performance concerning reticular patterns quantification is mainly challenged by false positives, due to their radiological similarity to vessel tree structures, thus reticular pattern identification and characterization has mostly benefited from the vessel tree removal stage. The reduced accuracy in ground glass pattern identification and characterization is attributed to its radiologic similarity with lung parenchyma, as well as partial volume effect and presence of noise. Fig. 4 is an illustrative example of the proposed system in a patient with normal LP where false-positive identifications of the system are mainly attributed to inaccurate vessel tree removal and the partial volume effect. To further improve differentiation between normal and ground glass pattern, an increased number of normal training patterns are required. This is a difficult task to achieve, taking into account that exposure to ionizing radiation must be justified.

Lung lobe segmentation is a further important step that should be considered in DPLDs systems, since lobar distribution of DPLDs patterns plays an important role in diagnosis, however, not dealt by our study [20].

Pixel-exact ground truth derivation is a tedious task, challenging the development and evaluation of such systems, thus development of graphical user interfaces providing effective editing tools is a necessity.

Furthermore, performance evaluation should consider comparison to inter and intraobserver variability on an augmented dataset.

V. CONCLUSION

An automated system for identification and characterization of interstitial lung disease, as depicted on MDCT scans is presented. The system is based on an optimized data preprocessing step to isolate LP and on a three-class k-NN classification approach, utilizing 3-D cooccurrence features to classify LP voxels into three categories: normal, ground glass, and reticular.

Preliminary results are promising, suggesting an accurate and reproducible system. Such systems are expected to assist radiologists in detection, characterization, and follow-up quantification of interstitial DPLDs.

ACKNOWLEDGMENT

The authors would like to thank Prof. A. P. Andonopoulos and Lect. D. Daoussis, Department of Internal Medicine, Division of Rheumatology, Medical School University of Patras, Patras, Greece, for providing the patient data.

REFERENCES

[1] I. C. Sluimer, M. Prokop, I. Hartmann, and B. van Ginneken, "Automated classification of hyperlucency, fibrosis, ground glass, solid, and focal lesions in high-resolution CT of the lung," *Med. Phys.*, vol. 33, no. 7, pp. 2610–2620, 2006.

[2] Z. A. Aziz, A. U. Wells, D. M. Hansell, S. J. Copley, S. R. Desai, S. M. Ellis, F. Gleeson, S. Grubnic, A. Nicholson, S. Padley, K. Pointon, J. Reynolds, R. Robertson, and M. Rubens, "HRCT diagnosis of diffuse parenchymal lung disease: Interobserver variation," *Thorax*, vol. 59, no. 6, pp. 506–511, 2004.

[3] F. Chabat, G.-Z. Yang, and D. M. Hansell, "Obstructive lung diseases: Texture classification for differentiation at CT," *Radiology*, vol. 228, no. 3, pp. 871–877, 2003.

[4] H.-U. Kauczor, K. Heitmann, C. P. Heussel, D. Marwede, T. Uthmann, and M. Thelen, "Automatic detection and quantification of ground-glass opacities on high-resolution CT using multiple neural networks: Comparison with a density mask," *Amer. J. Roentgenol.*, vol. 175, no. 5, pp. 1329–1334, 2000.

[5] I. C. Sluimer, P. F. van Waes, M. A. Viergever, and B. van Ginneken, "Computer-aided diagnosis in high resolution CT of the lungs," *Med. Phys.*, vol. 30, no. 12, pp. 3081–3090, 2003.

[6] Y. Uchiyama, S. Katsuragawa, H. Abe, J. Shiraishi, F. Li, Q. Li, C.-T. Zhang, C.-T. Zhang, and K. Doi, "Quantitative computerized analysis of diffuse lung disease in high-resolution computed tomography," *Med. Phys.*, vol. 30, no. 9, pp. 2440–2454, 2003.

[7] Y. Xu, E. J. R. van Beek, Y. Hwanjo, J. Guo, G. McLennan, and E. Hoffman, "Computer-aided classification of interstitial lung diseases via MDCT: 3-D adaptive multiple feature method (3-D AMFM)," *Acad. Radiol.*, vol. 13, no. 8, pp. 969–978, 2006.

[8] V. A. Zavaletta, B. J. Bartholmai, and R. A. Robb, "High resolution multidetector CT-aided tissue analysis and quantification of lung fibrosis," *Acad. Radiol*, vol. 14, no. 7, pp. 772–787, 2007.

[9] P. Korfiatis, A. Karahaliou, A. Kazantzi, C. Kalogeropoulou, and L. Costaridou, "Towards quantification of interstitial pneumonia patterns in lung multidetector CT," in *Proc. 8th IEEE Int. Conf. BioInf. BioEng. (BIBE 2008)*, pp. 1–5.

[10] K. Marten, V. Dicken, C. Kneitz, M. Hoehmann, W. Kenn, D. Hahn, and C. Engelke, "Computer-assisted quantification of interstitial lung disease associated with rheumatoid arthritis: Preliminary technical validation," *Eur. J. Radiol.*, vol. 19, no. 2, pp. 324–332, 2009.

[11] W. F. Sensakovic, S. G. Armato, A. Starkey, and P. Caliguiri, "Automated lung segmentation of diseased and artifact-corrupted magnetic resonance sections," *Med. Phys.*, vol. 33, no. 9, pp. 3085–3093, 2006.

[12] P. Korfiatis, S. Skiadopoulos, P. Sakellaropoulos, C. Kalogeropoulou, and L. Costaridou, "Combining 2-D wavelet edge highlighting and 3-D thresholding for lung segmentation in thin-slice CT," *Brit. J. Radiol.*, vol. 80, no. 960, pp. 996–1004, 2007.

[13] C. Zhou, H-.P. Chan, B. Shahiner, L. M. Hadjiiski, A. Chughtai, S. Patel, J. Wei, J. Ge, P. N. Cascade, and E. A. Kazerooni, "Automatic multiscale enhancement and segmentation of pulmonary vessels in CT pulmonary angiography images for CAD applications," *Med. Phys.*, vol. 34, no. 12, pp. 4567–4577, 2007.

[14] R. M. Haralick, K. Shanmugam, and I. H. Dinstein, "Textural features for image classification," *IEEE Trans. Syst., Man, Cybern.*, vol. SMC-3, no. 6, pp. 610–621, Nov. 1973.

[15] Y. Xu, M. Sonka, G. McLennan, J. Guo, and E. A. Hoffman, "MDCT-based 3-D texture classification of emphysema and early smoking related lung pathologies," *IEEE Trans. Medi. Imag.*, vol. 25, no. 4, pp. 464–475, Apr. 2006.

[16] K. Einslein, A. Ralston, and H. S. Wilf Eds, *Statistical Methods for Digital Computers*. New York: Wiley, 1977, pp. 76–94.

[17] P. Korfiatis, C. Kalogeropoulou, A. Karahaliou, A. Kazantzi, S. Skiadopoulos, and L. Costaridou, "Texture classification-based segmentation of lung affected by interstitial pneumonia in high-resolution CT," *Med. Phys.*, vol. 35, pp. 5290–302, 2008.

[18] I. Sluimer, M. Prokop, and B. van Ginneken, "Toward automated segmentation of the pathological lung in CT," *IEEE Trans. Med. Imag.*, vol. 24, no. 8, pp. 1025–1038, Aug. 2005.

[19] I. Sluimer, A. Schilham, M. Prokop, and B. van Ginneken, "Computer analysis of computed tomography scans of the lung: a survey," *IEEE Trans. Med. Imag.*, vol. 25, no. 4, pp. 385–405, Apr. 2006.

[20] T. Cover and P. Hart, "Nearest neighbor pattern classification," *IEEE Trans. Inf. Theory*, vol. 13, no. 1, pp. 21–27, Jan. 1967.

Panayiotis D. Korfiatis was born in Pyrgos, Greece, in 1983. He received the B.Sc. degree in physics and the M.Sc. degree in medical physics from the University of Patras, Patras, Greece, in 2004 and 2006, respectively. He is currently working toward the Ph.D. degree in the Department of Medical Physics, University of Patras.

His current research interests include 3-D image analysis techniques, pattern recognition, and computer-aided diagnosis methods.

Anna N. Karahaliou was born in Patras, Greece, in 1977. She received the B.Sc. degree in physics, the M.Sc. and the Ph.D. degrees in medical physics from the University of Patras, Patras, in 2001, 2003, and 2009, respectively.

Her research interests include medical image processing and analysis and pattern recognition.

Mrs. Karahaliou is recipient of the Best Student Paper Award in 2006 International Special Topic Conference on Information Technology Applications in Biomedicine.

Alexandra D. Kazantzi received the M.D. degree and the M.Sc. degree in biomedical sciences (molecular biology) from the School of Medicine, University of Patras, Patras, Greece, in 1998 and 2003, respectively. She is currently working toward the Ph.D. degree in the School of Medicine, University of Patras.

She completed her residency in radiology with the University Hospital of Patras and received the Radiologic Specialty in 2008. She is currently a Junior Radiologist with St. Andrews Hospital, Patras. Her research interests include thoracic radiology and medical imaging.

Christina Kalogeropoulou received the M.D. degree from the School of Medicine, University of Patras, Patras, Greece and the Ph.D. degree from the Department of Radiology, University Hospital of Patras, Patras.

She completed Radiology Residency from University Hospital of Patras. She is currently an Assistant Professor of Radiology with the University Hospital of Patras. Her research interests include cross-sectional imaging of chest and liver pathology and the design and evaluation of computer-aided diagnosis methods regarding the aforementioned anatomic areas.

Lena I. Costaridou received the B.Sc. degree in physics from the University of Patras, Patras, Greece, the M.Sc. degree in medical engineering from the Department of Electrical Engineering and Applied Sciences, George Washington University, Washington, DC, in 1979 and 1982, respectively, and the Ph.D. degree in medical physics from the University of Patras, in 1997.

She is currently an Assistant Professor with the Department of Medical Physics, School of Medicine, University of Patras. Her research interests include medical image processing & analysis with emphasis on tissue quantification and characterization in the frame of computer-assisted diagnosis systems, and quality of medical imaging systems. She is author/co-author of 60 articles in international refereed journals and more than 90 international conference papers, and reviewer for several international journals. She is the Editor of the book *Medical Image Analysis Methods* (CRC Press, 2005).